Pharmaceutical Sciences, 2024, 30(4), 444-455
doi:10.34172/PS.2024.9
https://ps.tbzmed.ac.ir/

Research Article

Improved Biological Impacts of Anti-EGFR Monoclonal Antibody in KRAS-Mutant Colorectal Cancer Cells by Silica-Coated Magnetic Nanoparticle Conjugation

Maedeh Yousefi[1], Hamed Farzi-Khajeh[2], Mostafa Akbarzadeh-Khiavi[2*], Azam Safary[3*], Khosro Adibkia[1,4]

[1]*Research Center for Pharmaceutical Nanotechnology, Biomedicine Institute, Tabriz University of Medical Sciences, Tabriz, Iran.*
[2]*Liver and Gastrointestinal Diseases Research Center, Tabriz University of Medical Sciences, Tabriz, Iran.*
[3]*Connective Tissue Diseases Research Center, Tabriz University of Medical Sciences, Tabriz, Iran.*
[4]*Department of Pharmaceutics, Faculty of Pharmacy, Tabriz University of Medical Sciences, Tabriz, Iran.*

Article Info

Article History:
Received: 2 Jan 2024
Accepted: 13 Mar 2024
ePublished: 6 Jul 2024

Keywords:
-Colorectal cancer
-EGFR
-KRAS mutant
-Magnetic nanoparticles
-PEGylation
-Reactive oxygen species

Abstract

Background: The therapeutic potential of epidermal growth factor receptor (EGFR) targeting in colorectal cancer (CRC) is hindered by the presence of KRAS codon 12 activating mutations, prevalent in approximately 25% of advanced CRC cases. This study investigates the role of reactive oxygen species (ROS) in conferring resistance to anti-EGFR monoclonal antibodies in KRAS mutant CRC cells, focusing on ROS-mediated apoptosis induction using cetuximab-PEGylated silica-coated magnetic nanoparticles (MNPs).

Methods: MNPs were synthesized and surface-coated with silica, followed by functionalization and stabilization with polyethylene glycol (PEG). Cetuximab (Cet) was covalently conjugated to generate EMNP-PEG-Cet. Structural and compositional analyses were performed using scanning electron microscopy (SEM), dynamic light scattering (DLS), UV-vis spectroscopy, and Fourier transform infrared (FTIR) analysis. Apoptosis induction, chromatin condensation, and ROS production were evaluated in KRAS mutant SW-480 CRC cells.

Results: Successful synthesis of EMNP-PEG-Cet was confirmed, revealing a particle size of 67 nm and a surface charge of -8.3 mV. The conjugate exhibited significant cytotoxicity against CRC cells, with notable apoptosis induction and ROS generation in EGFR-positive/KRAS mutant SW-480 cells, surpassing the effects observed with bare Cet and EMNP-PEG controls. The nuclear factor erythroid 2-related factor 2/Kelch-like ECH-related protein 1 (Nrf2-Kaep1) gene expression analysis by real-time PCR showed that cells treated with EMNP-PEG-Cet exhibited a noteworthy decrease in Nrf2 expression and a simultaneous increase in Keap1 expression compared to those treated with free Cet.

Conclusion: These findings highlight the potential of ROS-mediated apoptosis induction to enhance the cytotoxicity of Cet in EGFR-positive/KRAS mutant CRC cells, offering new avenues for overcoming drug resistance mechanisms in metastatic CRC.

Introduction

Colorectal cancer (CRC) is the third most prevalent cause of death worldwide. It arises from genetic mutations impacting oncogenes, tumor suppressors, and DNA repair-associated genes.[1] Various treatment avenues are available for managing CRC, including surgery, radiation therapy, chemotherapy, and emerging techniques like immunotherapy and targeted therapy.[2]

The heightened activation of the epidermal growth factor receptor (EGFR) signaling pathway significantly drives metastatic CRC development, establishing EGFR as a promising therapeutic target.[3,4] EGFR-targeted monoclonal antibodies (mAbs) like Cetuximab (Cet) have garnered attention for improving survival rates in metastatic CRC. However, their therapeutic response is hindered by various resistance mechanisms, including mutations in key RAS/RAF/PI3K genes, activation of the ERBB2/MET/IGF-1R pathway, increased EGFR ligands, alterations in EGF receptors, and notable changes within the tumor microenvironment.[5,6] Considering these challenges, ongoing research is focused on understanding and overcoming resistance mechanisms to develop more effective therapeutic options.[7]

Reactive oxygen species (ROS) play an important role in cancer biology, especially in CRC.[8] Cancer cells generally contain higher levels of ROS compared to normal cells due

*Corresponding Authors: Mostafa Akbarzadeh-Khiavi, E-mail: mostafaakbarzadehkhiavi@gmail.com & Azam Safary, E-mail: azamsafary@yahoo.com

to metabolic changes. This adaptation helps them develop antioxidant defenses, avoid apoptosis or ferroptosis pathways, and make them resistant to drugs.[4,9] The nuclear factor erythroid 2-related factor 2/Kelch-like ECH-related protein 1 (*Nrf2*/*Keap 1*) pathway is crucial in protecting cells from oxidative stress and inflammation.[8] Activation of this pathway induces detoxification, antioxidant activities, and anti-inflammatory effects in normal cells, while triggering apoptosis in cancer cells.[10] In response to varying levels of oxidative stress, cancer cells produce antioxidant enzymes like superoxide dismutase, catalase, and peroxiredoxins, making them susceptible to targeted elimination.[11,12] ROS-inducing approaches aim to increase the ROS level beyond the cytotoxic threshold, causing redox homeostasis disturbance in cancer cells and prompting them to undergo apoptosis. This vulnerability in cancer cells can be a promising foundation for developing selective therapeutic approaches.[13,14] The ROS-dependent apoptosis strategy shows promise in enhancing the effectiveness and customization of CRC treatments.[15]

Recent advances in pharmaceutical nanosystems have led to the development of secure and effective targeted drug delivery systems. The use of nanomaterials and nano-based drug delivery systems could significantly enhance cancer treatment by selectively inducing pathways within tumor cells, disrupting cellular balance, and damaging crucial cellular components.[16-19] In this regard, various systems have been developed, such as liposomes, niosomes, polymeric nanoparticles (NPs), micelles, gold, and iron oxide NPs.[20]

Magnetic nanoparticles (MNPs) have emerged as particularly promising in biomedical applications due to their magnetism, biocompatibility, and versatility in hyperthermia.[21-23] MNPs can be engineered to integrate multiple therapeutic functions, such as hyperthermia and drug delivery, or a combination of therapeutic and diagnostic functions, often referred to as theranostics. The synergistic effect of hyperthermia, coupled with the increased blood flow it induces, contributes to heightened drug concentration in the tumor area. As a result, intracellular drug uptake is augmented, and DNA damage and apoptosis are intensified.[24] Despite having promising features, MNPs face challenges such as aggregation at higher concentrations, which results in a reduced surface area. To address this issue, strategic functionalization with materials like polymers is required. This not only enhances the stability of the nanoparticles but also facilitates precise drug and gene delivery.[25-27]

MNPs are also prone to oxidation-reduction reactions due to their unique physical and chemical properties.[28] Numerous studies have demonstrated that MNPs can induce dose-dependent oxidative stress by depleting glutathione and inducing ROS production, disrupting the balance between oxidation and antioxidant systems.[29] This oxidative stress can lead to lipid peroxidation, DNA and protein damage, and dysregulation of signaling pathways. In conditions of high ROS content, pathways involving *Nrf2* and P38 MAPK are commonly activated to generate antioxidants and alleviate oxidative stress.[30] Moreover, elevated ROS levels within mitochondria result in decreased ATP production, disrupting the tricarboxylic acid (TCA) cycle and reducing cardiolipin levels, which coordinates inflammatory metabolic reprogramming.[31-33] Evidence suggests that ROS originating from mitochondria may contribute to apoptosis triggered by Tumor Necrosis Factor-alpha (TNF-α) and Interleukin (IL)-1 beta (IL-1β). Excessive ROS generation initiates a cascade of pro-inflammatory cytokines and mediators via redox-sensitive MAPK and Nuclear factor kappa B (NF-κB) signaling pathways, regulating the transcription of inflammatory genes such as IL-1, IL-8, and TNF-α.[33]

The current study aimed to address a strategy for overcoming drug resistance in KRAS-mutated CRC cells by conjugating PEGylated MNPs with Cet to develop EMNP-PEG-Cet nanobiomedicine. The study evaluated the ability of these conjugates to induce ROS-mediated apoptosis in KRAS-mutated cells and provided insights into overcoming drug resistance in metastatic CRC.

Methods

Materials

Antibody Cet was purchased from Merck, Inc. (Merck, Germany). RPMI 1640 medium, fetal bovine serum (FBS), and 3– (4,5 dimethylthiazol-2-yl)-2,5-diphenyltetrazolium bromide (MTT) were obtained from Sigma-Aldrich (St Louis, MO). Chemicals, including N-hydroxyl succinimide (NHS), $FeCl_3.6H_2O$, $FeCl_2.4H_2O$, 1-Ethyl-3-(3-dimethylaminopropyl)-carbodiimide (EDC), and phosphate-buffered saline (PBS) were provided from Sigma-Aldrich Company (Munich, Germany). Annexin V-FITC apoptosis detection kit was obtained from eBiosciences (MA, United States).

Synthesis and characterization of nanoconjugates

MNPs preparation

An alkaline co-precipitation method under argon conditions was employed to synthesize MNPs.[34] Initially, a round bottom flask containing 6.8 g of $FeCl_3.6H_2O$ and 2.5 g of $FeCl_2.4H_2O$ in 300 mL of deionized water was stirred with a magnetic stirrer for 20 minutes at room temperature (RT). To synthesize MNPs, the pH of the reaction mixture was gradually raised to 12 by adding ammonia solution dropwise (~ 70 mL) with consistent and vigorous stirring. Subsequently, we separated the resulting black sediment by centrifugation for 10 minutes at 10000 rpm. To remove any unreacted ions, several washing steps with water and ethanol were conducted. Finally, the MNPs were dried under a vacuum at 50 °C overnight.

Silica-coated MNPs (SMNPs) preparation

To create silica-coated MNPs (SMNPs), we employed a modified version of a previously published method,[34] using tetraethyl orthosilicate (TEOS) as the coating agent. Initially, 5.0 g of MNPs was mixed with ethanol

and deionized water (300 mL) in a 4:1 volume ratio. The mixture underwent sonication in a water bath sonicator to ensure a homogeneous suspension. Afterward, the pH was raised to 10 by adding an ammonia solution. Subsequently, TEOS (10 mL) was slowly dripped into the solution, which was then stirred with a mechanical stirrer in an argon atmosphere for 5 hours at 60 °C. Upon completion of the coating process, the SMNPs were separated using an external magnet and subjected to three washing steps with a solution of ethanol and deionized water. Finally, the obtained dark brown SMNPs were dried under vacuum conditions at 50 °C for 18 hours, forming well-defined silica-coated magnetic NPs with desirable properties for various applications.

Surface functionalize of SMNP (EMNPs)

To functionalize the SMNPs, an excess of (3-Glycidyloxypropyl) trimethoxysilane (GPTMS) (7.5 mL) and 3 mL of triethylamine (TEA) were added to a mixture containing 3.0 g of dried SMNPs and 300 mL of dry toluene. Then, the mixture was agitated using a mechanical stirrer for 48 hours at 90 °C under an argon atmosphere. Afterward, we introduced a chloropropyl functional group to the SMNPs and performed magnetic separation. The epoxy-activated SMNPs (EMNPs) were washed twice with toluene, twice with deionized water, and twice with ethanol before being dried at 50 °C overnight.

PEGylation procedure of EMNPs

In this study, the EMNPs were surface-modified with functional carboxyl groups to enhance their stability and biocompatibility. We prepared a solution containing 1.036 mg (0.0054 moL) of EMNPs in 10 mL of double-distilled water to achieve this modification. To create the PEGylation agent, HS-PEG-COOH (1 mg, 0.5 mol) was dissolved in double-distilled water (1 mL). Subsequently, the PEGylation agent was added to the EMNPs solution, and the mixture underwent vortexing to achieve thorough blending. The reaction was allowed to proceed overnight at RT. After the PEGylation process, the modified EMNPs (EMNP-PEG) underwent characterization using several techniques.

Conjugation of EMNP-PEG with Cet (EMNP-PEG-Cet)

To covalently bind EMNP-PEG to Cet, we utilized the EDC-NHS covalent binding method. Initially, a 2 mL solution of EMNP-PEG (0.21 mg, 0.62 nmoL) was prepared and mixed with EDC (30 µL, 400 mM) and NHS (30 µL, 120 mM) to activate the carboxyl groups on the surface of MNPs. The mixture was then incubated at RT for 2 hours to facilitate the formation of amine-reactive ester intermediates. Subsequently, Cet (20 µL, 0.1 mg, 0.68 nmol) was added to the reaction and subjected to a 3 hours incubation at 4 °C, with continuous shaking. Subsequently, the EMNP-PEG-Cet nanoconjugates were recovered through centrifugation at 10,000 rpm and washed three times with PBS buffer.

Efficiency of Cet loading/unloading on EMNP-PEG

Quantification of Cet conjugation was conducted utilizing a bicinchoninic acid (BCA) protein assay kit to determine the total mAb content in the supernatant. Subsequently, the mAb loading percentage was calculated using the provided equation, with unloaded protein and protein loaded on NPs expressed in mg/mL.

mAbs Loading %=[Total mAb-Unloaded mAb]/[Total mAb] ×100

Physicochemical characterization of EMNP-PEG-Cet

The characterizations of NPs were determined using Fourier-transform infrared spectroscopy (FTIR). The zeta potential and dynamic light scattering (DLS) of the designed nanoconjugates (EMNP-PEG-Cet) were investigated with Nanotrac WaveTM (Microtrac, USA). Additionally, the size and morphology of the nanoconjugate were determined through Scanning electron microscopy (SEM) (TeScan Mira-3, Czech Republic).

EMNP-PEG-Cet binding affinity evaluation

The binding affinity of EMNP-PEG-Cet to EGFR receptors was determined using Western blot analysis. Concisely, the SW-480 cells were lysed using RIPA buffer and then subjected to electrophoresis on a 12% polyacrylamide gel for separation. Subsequently, the protein bands were transferred onto a PVDF membrane (polyvinylidene fluoride) to initiate the Western blotting phase. A solution containing 5% BSA within the TBST buffer (20 mM Tris, 150 mM sodium chloride, and 0.05% Tween-20) was employed to prevent non-specific binding occurrences. This step involved an overnight incubation of the PVDF membrane at 4 °C. Then, the primary antibody (EMNP-PEG-Cet nanostructure) was allowed to incubate on the membrane for 1.5 hours at RT. After that, the membrane underwent a 5-minute wash with TBST buffer at RT to eliminate any unbound primary antibody. Subsequently, the secondary antibody (anti-human IgG-HRP) was prepared, with a ratio of 1:3000 in a buffer containing 3% BSA, and it was applied to the membrane for 1 hour at RT. The ultimate step involved visualizing and analyzing the protein bands using the BM chemiluminescence kit.

Cellular cytotoxicity assay

The SW-480 cell line was sourced from the Pasteur Institute (Tehran, Iran). The cytotoxic impact of EMNP-PEG-Cet was examined on SW-480 cells via the MTT assay. SW-480 cells with a seeding density of 1.0×10^4 cells per well were grown in 96-well microplates. Subsequently, the cells were exposed to various concentrations (10, 25, 50, 75, 100, and 200 µg/mL) of EMNP-PEG-Cet, Cet, EMNPs, and EMNP-PEG for 24, 48, and 72 hours. Following the incubation periods, the culture medium was replaced with fresh MTT reagent (200 µL, 2 mg/mL) and incubated for 4 hours. The formazan crystals were dissolved in 200 µL of dimethyl sulfoxide (DMSO) after removing the MTT reagent. Then, the optical density at 570 nm was measured using

a BioTeck Elisa reader (model elx808, BioTeck, Winooski, VT, USA). The IC_{50} dose was determined using GraphPad Prism software.

Nuclear morphology assay by DAPI staining

The impact of EMNP-PEG-Cet nanoconjugates on cell nuclei morphology was assessed through DAPI (4′,6-diamidino-2-phenylindole) staining. Initial cell seeding was conducted in a 6-well microplate, with cells introduced at a 1.0×10^5 cells/cm^2 density. Following 24 hours incubation period at 37 °C, the cells underwent treatment with an IC_{50} dose of EMNP-PEG-Cet, Cet, EMNPs, and EMNP-PEG for an additional 24 hours. Following three washes with PBS, the cells were fixed by immersing them in 4% ice-cold paraformaldehyde (PFA) for a 20 minute incubation at 37 °C. Afterward, another PBS wash was carried out, followed by a 5 minute permeabilization step using 0.1% Triton-X-100. The cells were then subjected to another round of PBS washing and exposed to a 0.1% DAPI solution for 6 minutes for nuclear staining. Finally, cells were washed using Triton X-100 (0.1%) within PBS and subsequently imaged using the Cytation 5 imaging system (Biotek, Winooski, USA).

Apoptosis assay by annexin V/PI staining

The SW-480 cells were seeded at 1.0×10^5 cells per well. After 24 hours, cells were treated with compounds, including Cet, EMNPs, EMNP-PEG, and EMNP-PEG-Cet, all at their IC_{50} concentrations. The cells were then analyzed using an annexin V kit, following the guidelines provided by the manufacturer. Flow cytometry was used to analyze the cells, with a BD FACSCalibur™ instrument (Becton Dickinson, Franklin Lakes, NJ, USA) being employed for this purpose.

ROS detection by DCFH-DA assay

To assess the production of ROS, a fluorescent probe, 2′,7′ dichlorodihydrofluorescein diacetate (DCFH-DA) was employed. DCFH-DA undergoes hydrolysis via intracellular esterase, forming DCFH. This assay evaluates treatment effects on ROS levels, providing insights into their efficacy against oxidative stress in cancer cells. ROS quantification relies on DCFH-DA transforming into DCF, serving as a ROS presence indicator.[35] Briefly, the SW-480 cells were initially seeded at a density of 1.5×10^5 cells/well in 6-well plates and cultivated for 24 hours. Subsequently, the cells underwent treatment with IC_{50} dose of free Cet, EMNP-PEG, and EMNP-PEG-Cet, for 24 hours. Then, the cells were incubated with 400 µL of medium containing DCFH-DA (5 µM) at 37 °C for 30 minutes. After that, the live imaging system Cytation 5 (Biotek, Winooski, USA) was employed to measure the fluorescence intensity, indicative of ROS production, supplemented by flow cytometry analysis.

Oxidative stress gene expression assay

Briefly, SW-480 cells were cultured at a density of 1×10^5 cells/well in 6-well plates and incubated for 24 hours. Subsequently, the cells were treated with the IC_{50} dose of free Cet, EMNP-PEG, and EMNP-PEG-Cet for an additional 24 hours. Total cellular RNA was then extracted from the treated SW-480 cells using the TRIZOL method, and cDNA was synthesized using the Takara Primescript RT reagent kit, following the kit's instructions. The qRT-PCR analysis was performed utilizing the Maxima SYBR Green/ROX qPCR master mix and the Bio-Rad iQ5 system (BioRad Laboratories Inc., Hercules, USA). Specific primers for *Nrf2* and *Keap1* genes were designed using the NCBI primer design online software and validated through the NCBI primer BLAST tool. To standardize the cycle threshold (CT) values, glyceraldehyde-3-phosphate dehydrogenase (GAPDH) served as the housekeeping gene.

Statistical analysis

The data were presented as mean values ± standard deviation (SD), and statistical significance was considered at $P < 0.05$. The evaluation was conducted using analysis of variance (ANOVA) and Student's t-test. Statistical analysis was performed using SPSS Version 18.0 software.

Results

Characterization of EMNPs-PEG-Cet nanoconjugate

A series of three main steps were conducted to fabricate the engineered EMNP-PEG-Cet. Initially, EMNPs were synthesized using the alkaline co-precipitation method. Next, the EMNPs were modified with HS-PEG-COOH. Finally, the conjugation of Cet to EMNPs-PEG was accomplished using EDC/NHS under carefully controlled conditions. The FTIR spectrum (Figure 1) of the EMNPs exhibited a prominent absorption band at 569 cm^{-1}, attributable to the stretching of the Fe-O bond. Meanwhile, in the FTIR spectrum of SMNPs, a broad peak observed at 1000–1100 cm^{-1} indicated the presence of Si-O-Si and Si-O-H stretching vibrations. Furthermore, Figure 1 revealed a characteristic peak at 1615 cm^{-1}, attributable to the stretching of the COOH group in the PEG coating. Additionally, the bending vibrations of the aliphatic -CH2- and O-H groups are observed at 2912 cm^{-1} and 3200-3450, respectively, in the PEG coating. Moreover, the DLS method was employed to ascertain the mean particle size of the different synthesized components. The DLS analysis revealed sizes of approximately 43 nm for EMNPs (PDI=0.421), 51 nm for EMNP-PEG (PDI=0.239), and 67 nm for EMNP-PEG-Cet (PDI=0.537) (Figure 2A). Zeta potential measurements were conducted to evaluate the surface potential of the samples. The results indicated an initial negative charge of approximately -18.1 mV on the surface of unconjugated EMNPs. Coating with PEG and Cet resulted in zeta potential enhancements to -13.6 mV and -8.3 mV, respectively, affirming the success of the conjugation process. A typical SEM analysis of EMNP-PEG-Cet exposed a spherical morphology characterized by a smaller dimension of roughly 45 nm, aligning closely

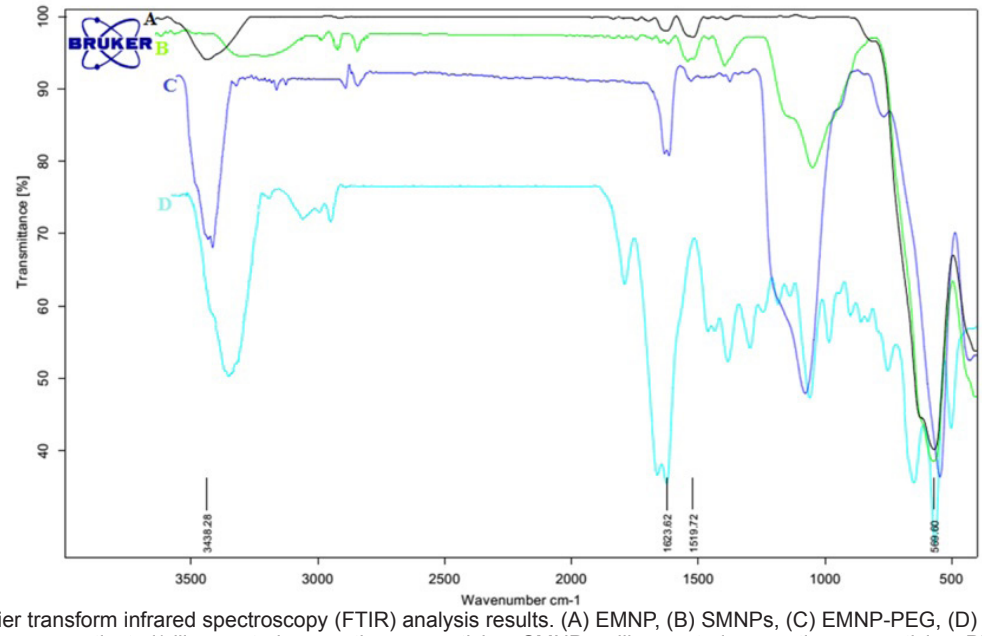

Figure 1. Fourier transform infrared spectroscopy (FTIR) analysis results. (A) EMNP, (B) SMNPs, (C) EMNP-PEG, (D) EMNP-PEG-Cet. EMNP: EMNP: epoxy-activated/silica-coated magnetic nanoparticles; SMNPs: silica-coated magnetic nanoparticles; PEG: polyethylene glycol; Cet: Cetuximab.

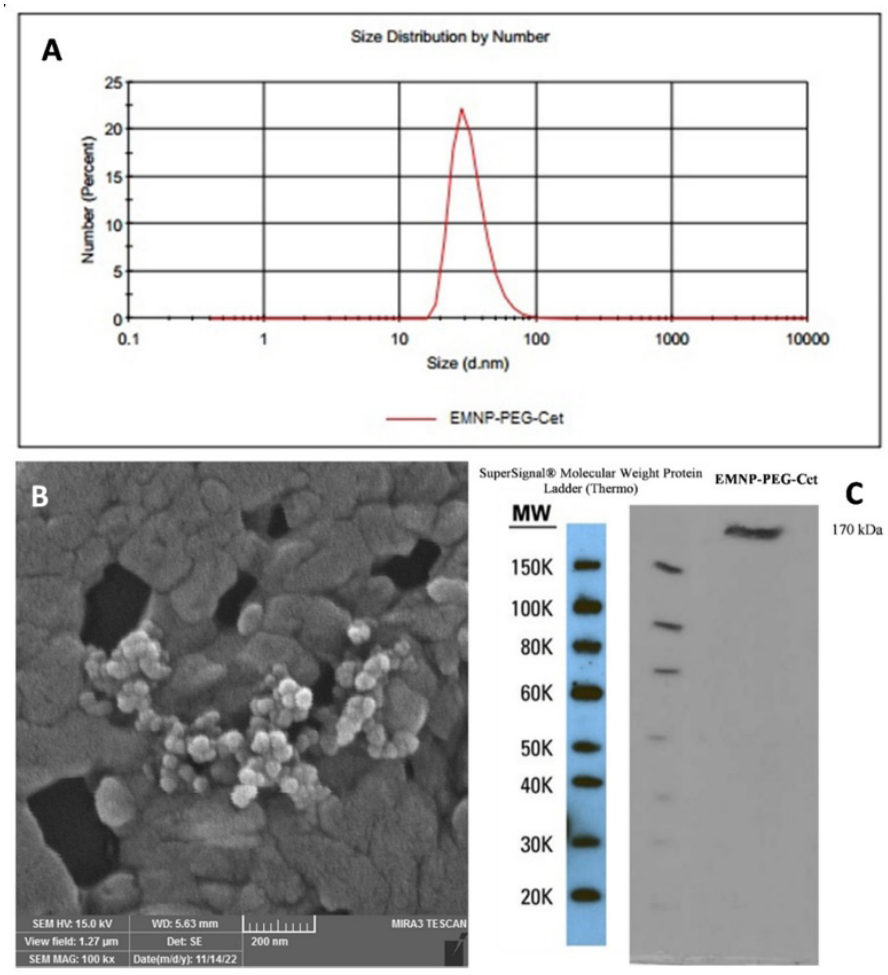

Figure 2. EMNP-PEG-Cet nanoconjugate physicochemical characterization. (A) Dynamic light scattering (DLS) measurement of EMNP-PEG-Cet. (B) Morphological analysis of EMNP-PEG-Cet by Scanning electron microscope (SEM). (C) Activity assay of the EMNP-PEG-Cet by Western blot. PDI: Polydispersity index; EMNP: epoxy-activated/silica-coated magnetic nanoparticles; PEG: Polyethylene glycol; Cet: Cetuximab.

with the DLS findings (Figure 2B). We assessed the activity of EMNP-PEG-Cet through Western blotting. These results conclusively demonstrated the complete binding activity of EMNP-PEG-Cet, confirming its functional binding activity against EGFR (Figure 2C). Additionally, a BCA kit assay was utilized to evaluate the yield of enzyme conjugation, estimated at approximately 81%.

Cytotoxic evaluation of EMNP-PEG-Cet

The cytotoxic effects of different concentrations of free Cet, EMNPs, EMNP-PEG, and EMNP-PEG-Cet were evaluated on SW-480 cells at 24, 48, and 72-hour intervals using MTT assays. The results indicated that treatment with EMNPs and EMNP-PEG at concentrations ranging from 10-200 µg/mL did not cause a significant reduction in cell viability compared to the untreated control group across all time points ($P > 0.05$) (Figure 3A, B, and C). However, the exposure of SW-480 cells to various concentrations of Cet and EMNP-PEG-Cet (10-200 µg/mL) resulted in a significant reduction of cell viability. The IC_{50} values for Cet-treated SW-480 cells were 173, 140, and 136 µg/mL after 24, 48 and 72 hours, respectively. The IC_{50} values for EMNP-PEG-Cet treated cells were determined as 132, 93, and 58 µg/mL in the same intervals, respectively (Figure 3D).

DAPI staining assay

We conducted DAPI staining to examine the impact of free Cet, EMNP-PEG, and EMNP-PEG-Cet on chromatin condensation and DNA fragmentation in SW-480 cells. Our findings showed that the EMNP-PEG-Cet treatment had a more significant impact on the shape of cell nuclei than the other treatments (Figure 4). These results confirmed that EMNP-PEG-Cet has a higher apoptotic effect, leading to increased levels of chromatin condensation and DNA fragmentation.

Cell apoptosis analysis by Annexin V

The apoptosis assay results (Figure 5) revealed a significant induction of both early (11.09%) and late (19.11%) apoptosis in the treated SW-480 cells by the EMPN-PEG-Cet nanostructure (Figure 5E). In contrast, the apoptosis rate in cells treated with free Cet was only 2.74% for early apoptosis and 7.14% for late apoptosis (Figure 5D). Similarly, cells treated with EMNPs-PEG displayed an apoptosis rate of approximately 1.2% for early apoptosis and 2.98% for late apoptosis (Figure 5C).

ROS production assay

In the present study, we investigated the impact of EMNP-PEG, EMNP-PEG-Cet, and free Cet on intracellular ROS production, employing the DCHF-DA assay through cell imaging and flow cytometry methods. Our findings revealed that the fluorescence intensity was significantly higher in cells treated with EMNP-PEG-Cet than those treated with EMNP-PEG or free Cet, as demonstrated in Figure 6.

ROS-related gene expression

Real-time PCR analysis showed that the expression levels

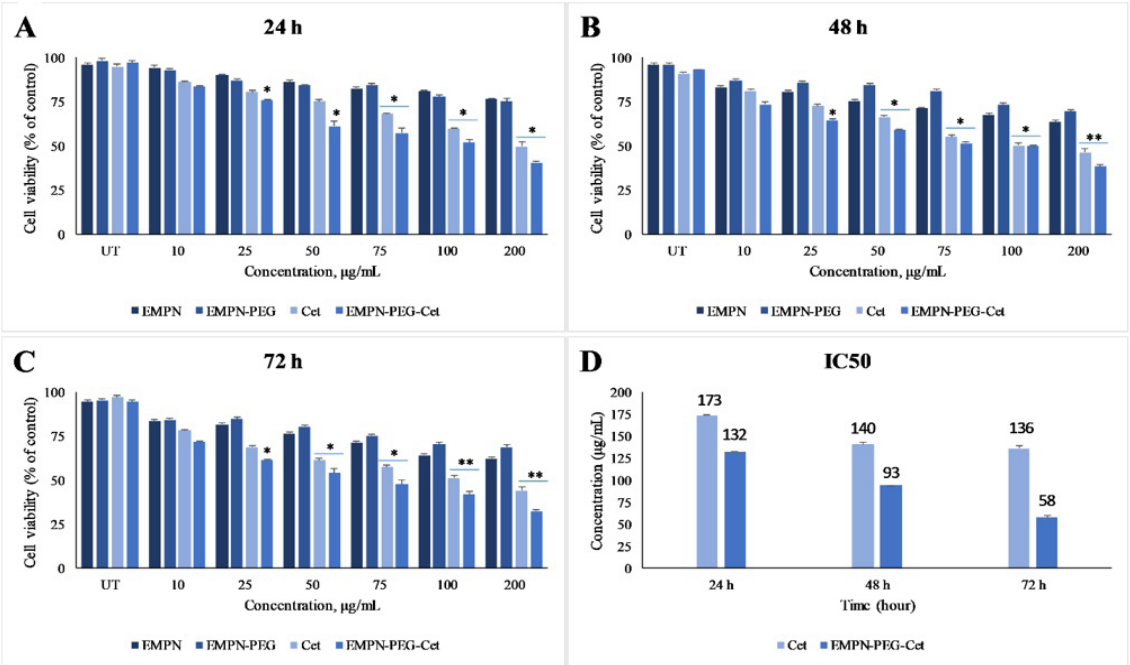

Figure 3. Cell viability assessment of the engineered EMNP-PEG-Cet nanoconjugate on SW-480 CRC cells. (A, B, and C) Cell viability assay of cells treated with EMNPs, EMNP-PEG, free Cet, and EMNP-PEG-Cet at various concentrations (10, 25, 50, 75, 100, and 200 µg/mL) and time points (24, 48, and 72 h). (D) Comparative IC_{50} values of Cet and EMNP-PEG-Cet nanoconjugate in SW-480 cells after 24, 48, and 78 h incubation. The data shown represent means ± SD from three independent experiments. EMNP: epoxy-activated/silica-coated magnetic nanoparticles; PEG: Polyethylene glycol; Cet: Cetuximab; UT: Untreated control cells. Indicates significant difference in comparison to control group (*$p < 0.05$ and **$p < 0.01$).

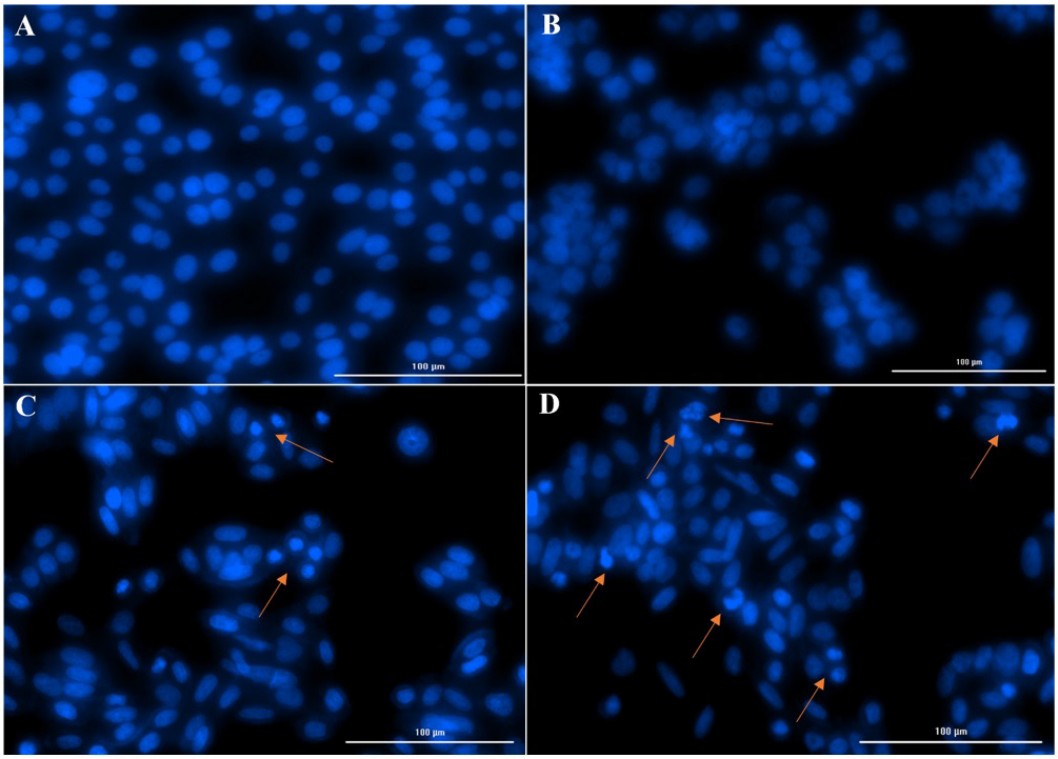

Figure 4. Assessing nucleus morphological changes in treated SW-480 cells through DAPI staining. (A) Untreated cells, (B) cells treated with EMNPs-PEG, (C) cells treated with free Cet, and (D) cells treated with EMNP-PEG-Cet. EMNP: epoxy-activated/silica-coated magnetic nanoparticles; PEG: Polyethylene glycol; Cet: Cetuximab. Red arrow: Chromatin condensation.

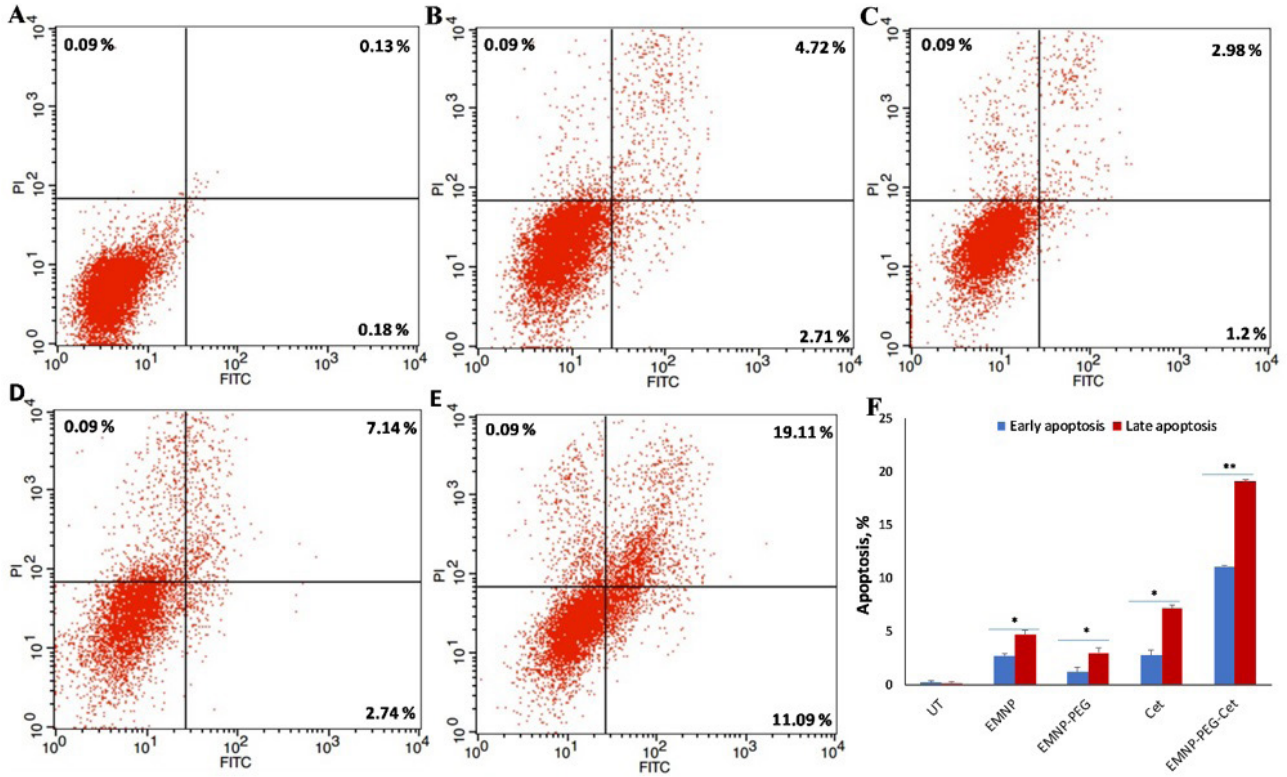

Figure 5. Evaluating apoptosis in SW-480 CRC cells treated with engineered EMNP-PEG-Cet nanoconjugate by annexin V-FITC/PI. (A) Untreated cells, (B) cells treated with EMNPs, (C) cells treated with EMNP-PEG, (D) cells treated with Cet, (E) cells treated with EMNP-PEG-Cet, and (F) the early and late apoptosis rate of cells after 24 h treatment with EMNP, EMNP-PEG, free Cet, and EMNP-PEG-Cet. EMNP: epoxy-activated/silica-coated magnetic nanoparticles; Cet: Cetuximab; PEG: Polyethylene glycol; UT: Untreated control cells. Indicates the significant difference compared to the control group (*$p < 0.05$ and **$p < 0.01$).

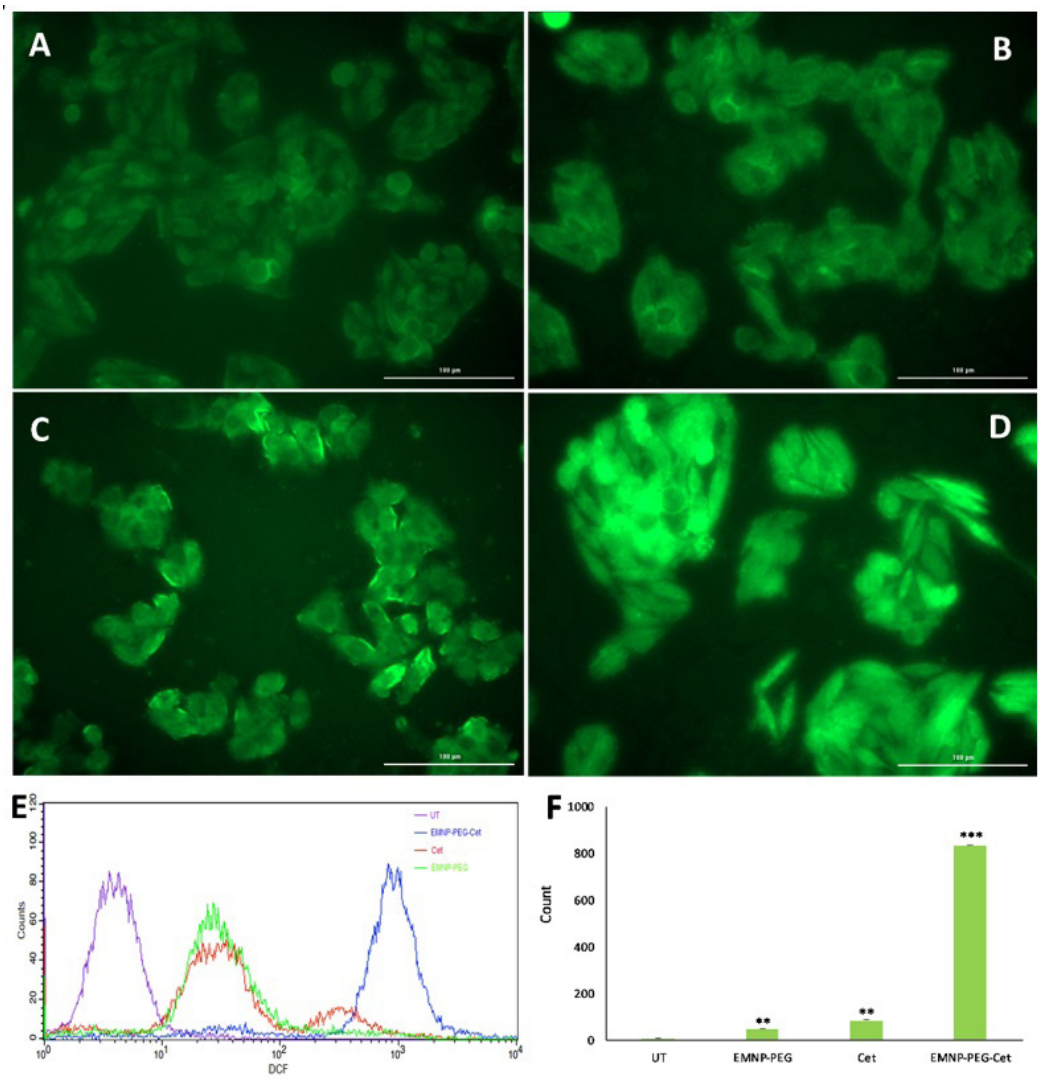

Figure 6. Assessing ROS production in SW-480 cells using DCHF-DA fluorescent dye. (A) Untreated cells, (B) cells treated with EMNP-PEG, (C) cells treated with free Cet, and (D) cells treated with EMNP-PEG-Cet. (E) Flow cytometry analysis of ROS generation in cells treated with IC_{50} of EMNPs-PEG, free Cet, and EMNP-PEG-Cet. (F) The rate of DCF intensity in the treated cells. DCHF-DA: 2,7 dichlorodihydrofluorescein diacetate; EMNP: epoxy-activated/silica-coated magnetic nanoparticles; PEG: Polyethylene glycol; Cet: Cetuximab; UT: Untreated control cells.

of *Nrf2* significantly decreased in SW-480 cells treated with EMNP-PEG-Cet ($p < 0.001$). Conversely, the expression of the *Keap1* gene significantly increased compared to untreated control cells. The use of free Cet led to an increase in *Keap1* expression ($p < 0.05$), accompanied by a significant decrease in *Nrf2* expression ($p < 0.05$). In the presence of EMNP-PEG, the expression of *Keap1* showed a slight change, while decreases were observed in *Nrf2* expression ($p < 0.05$) compared to untreated control cells.

Discussion

ROS play a dual role in cancer cell metabolism, serving as signals for cell proliferation at low to moderate levels and triggering cell death at high levels.[36] Recently, therapeutic strategies targeting ROS production have emerged to disrupt the ROS adaptation of cancer cells. These approaches hold significant promise for cancer therapy by increasing ROS levels, inducing oxidative stress, and initiating ROS-dependent apoptosis. It has been emphasized that mAbs exploit elevated ROS levels to efficiently induce cell demise.[15] Furthermore, preclinical studies have demonstrated the selective efficacy of ROS enhancers, particularly in CRC cells, surpassing the oxidative stress toxicity threshold. In this context, the combination of targeted nanoconjugates with ROS-mediated therapy shows promise for enhancing cancer treatment while minimizing harm to healthy cells.[4] In the current study, we investigated the potential of EMNP-PEG-Cet nanoconjugate to induce ROS-dependent apoptosis in SW-480 CRC cells. Characterization of the nanoformulated EMNP-PEG-Cet revealed an increase in particle size from 43 to 67 nm, accompanied by a shift in surface charge from -18.1 mV to -8.3 mV. Importantly, a clear correlation was established between the size of nanocarriers, their zeta potential, and their ability to interact with and penetrate cancer cells.[37] The SEM image of EMNP-PEG-Cet displayed a spherical shape,

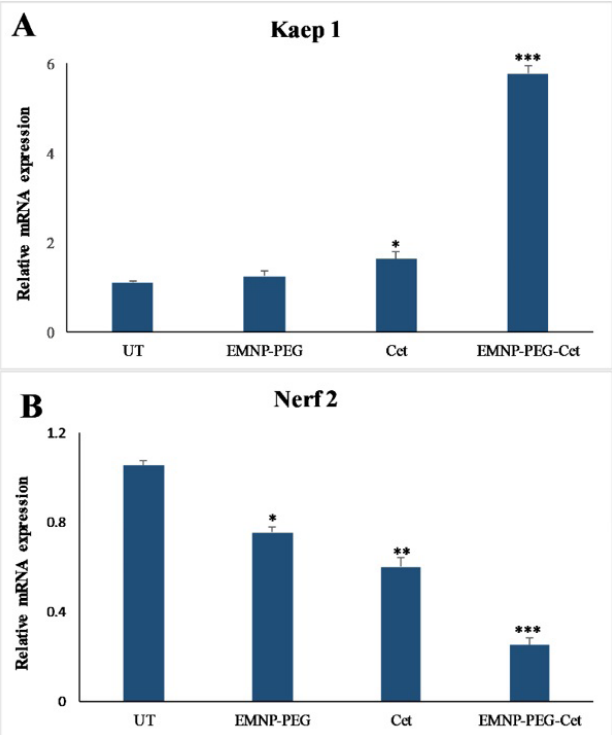

Figure 7. Expression analysis of ROS-related genes in the treated SW-480 cells by EMPN-PEG-cet via real-time PCR. (A) *Kaep1*, and (B) *Nrf2* expression ratios in the treated cells with EMNPs-PEG, free Cet, and EMNP-PEG-Cet. GAPDH was used as a housekeeping gene. Ct values were normalized using the Pfaffl method, and the results are presented as the mean values of independent triplicates (mean ± SD). EMNP: epoxy-activated/silica-coated magnetic nanoparticles; Cet: Cetuximab; PEG: Polyethylene glycol; UT: Untreated control cells. Indicates the significant difference compared to the control group (*p < 0.05, **p < 0.01 and ***p < 0.001).

corroborating the DLS results with a relatively smaller size. The slight variance between the DLS and SEM findings can be attributed to several factors. Firstly, SEM analyses involve dried NPs, whereas DLS analysis employs solvated NPs, leading to variations in observed sizes. Secondly, SEM analyses provide number-average diameter measurements, whereas DLS examinations yield intensity-weighted diameter measurements (hydrodynamic diameter).[38] The loading of Cet on NPs was approximately 81%. In Figure 3, EMNP-PEG-Cet displayed increased toxicity in a concentration- and time-dependent manner, with decreasing IC_{50} values over time. However, under the same conditions, EMNPs and EMPNs-PEG did not exhibit significant inhibitory effects on SW-480 cells. Mu *et al.*[39] demonstrated that both EGFR mAb-SPIONs (with a size of 161.5 nm) and SPIONs (with a size of 71.4 nm) had no significant impact on the viability of human liver normal HL-7702 cells and human endothelial ECV 304 cells.

Apoptosis is closely linked to changes in chromatin condensation and nuclear morphology. Upon exposure to EMNP-PEG-Cet and free Cet, detectable alterations were observed in the nuclei of SW-480 cells (Figure 4). Annexin V/PI staining was employed to assess cellular apoptosis, a sensitive method capable of detecting both early and late stages of apoptosis.[40] As shown in Figure 5E, the apoptosis assessment revealed that approximately 31% of cells treated with EMNP-PEG-Cet exhibited FITC/PI-positive features, indicating the translocation of cell surface phosphatidylserine, which compromises membrane integrity. In contrast, Cet-treated cells showed a lower apoptosis rate of about 10%, possibly due to the inherent KRAS-mutant resistance observed in SW-480 cells. Similar findings were reported by Tseng *et al.*,[41] demonstrating a significant increase in apoptosis in EGFR-overexpressing cell lines, such as epidermal carcinoma A431 cells and 32D/EGFR cells, after 24 hours of exposure to Cet-PEG-dexSPIONs compared to Cet treatment alone. However, their nanocomplex had different attributes from our formulation, particularly in composition. Their construct consisted of superparamagnetic NPs enveloped with dextran and conjugated to Cet (referred to as Cet-PEG-dexSPIONs), utilizing PEG as a bridging agent. Importantly, their nanoparticle configuration exhibited a size of approximately 91 nm with a zeta potential of -21.9 mV, distinctly more negative than the dextran-coated SPIONs with a zeta potential of -7.31 mV, thus establishing a clear distinction between their nanostructure and that utilized in the current study.

Numerous studies have highlighted elevated levels of ROS in cancer tissues compared to their normal cell counterparts.[17] ROS generation is often linked to the activation of pro-tumorigenic signaling pathways, promoting cell survival, proliferation, and inducing DNA damage and genetic instability.[42] Conversely, heightened ROS levels have shown the potential to trigger anti-tumorigenic signaling pathways, leading to tumor cell death through oxidative stress mechanisms. Notably, tumor cells possess adaptive mechanisms to cope with elevated ROS levels by upregulating antioxidant proteins, thus mitigating oxidative stress and preserving pro-tumorigenic signaling, which ultimately contributes to resistance against apoptosis.[17] Therefore, strategically targeting ROS holds promise as a therapeutic approach for cancer treatment, especially considering the distinct redox imbalance observed in cancer cells compared to normal cells.[5,43] In this study, the DCFH-DA hydrolysis assay revealed a significant increase in DCF fluorescence intensity in cells treated with EMNP-PEG-Cet compared to those treated with EMNP-PEG and free Cet (Figure 6). Cancer cells tend to maintain slightly elevated ROS levels compared to normal cells.[44] Furthermore, the observed effect of MNPs acting as redox catalysts amplifies lipid peroxidation and enhances ROS production.[45] However, a comprehensive understanding of this mechanism requires further exploration through extended studies. The pivotal role of Nrf2 in various cellular pathways has made this gene as a viable and promising target in CRC treatment. Numerous studies have been conducted to inhibit the Nrf2 antioxidant pathway, highlighting its significance in cancer therapy.[46,47] Intervening with the upstream regulators or downstream effectors of *Nrf2* signaling holds potential

for significant anticancer effects.[48] In this context, our study showed the therapeutic efficacy of a modified mAb, which mediates the downmodulation of the *Nrf2* signaling pathway in the SW-480 cell line. Analysis of *Nrf2-Kaep1* gene expression revealed a noteworthy decrease in *Nrf2* expression and a simultaneous increase in *Keap1* expression in cells treated with EMNP-PEG-Cet compared to those treated with free Cet alone. This underscores the promising therapeutic potential of targeting the *Nrf2* pathway for CRC treatment. Similar outcomes have been observed with combined exposure to Cet and RAS-selective lethal 3 (RSL3) in the KRAS-mutant CRC cell line.[6] Our finding suggests that the EMNP-PEG-Cet nanobiosystem not only inhibits the *Nrf2-Keap1* antioxidant pathway but also significantly increases the toxic accumulation of ROS, culminating in a profound induction of apoptosis in the treated SW-480 cells.

Overall, combining EMNPs and Cet could enhance the antitumor activity of mAbs by triggering ROS-mediated apoptosis in resistant cancer cells. The synergistic interaction between EMNPs and Cet leads to a significant increase in ROS production, suggesting that intracellular ROS formation plays a pivotal role in the cytotoxic effects exerted by EMNP-PEG-Cet on SW-480 cells. This mechanism likely involves DNA damage and other harmful effects, disrupting intracellular homeostasis and ultimately leading to cell toxicity and apoptosis. These findings propose a promising strategy to overcome the inherent resistance of KRAS-mutant cells to Cet by stimulating ROS production and suppressing the *Nrf2*-dependent antioxidant response in cancer cells using the newly developed EMNP-PEG-Cet nanoconjugate.

However, it is important to acknowledge potential limitations that could hinder the clinical translation of ROS-mediated interventions. The efficacy of such interventions during prolonged systemic administration may be compromised due to challenges related to biodegradability and biocompatibility. Additionally, a thorough understanding of the complex interplay between ROS-mediated nanoconjugates, their pharmacokinetics, and their impact on human physiology is essential for their eventual integration into clinical therapeutic protocols.

Conclusion

In conclusion, while EGFR-targeted therapies like Cet initially showed promise, the emergence of drug resistance mechanisms in cancer cells has prompted the exploration of alternative approaches. The intricate role of ROS in cancer cell metabolism has garnered significant attention, as ROS serve as dual regulators influencing both cell proliferation and cell death induction. This multifaceted role has spurred the development of innovative strategies aimed at manipulating ROS to enhance cancer treatment. Our study presents a unique approach by employing smart nanoconjugates, specifically integrating PEGylated EMNPs with Cet. This engineered nanobiosystem demonstrates strategic synergy capable of initiating ROS-dependent apoptosis within KRAS-mutant SW-480 cells. In summary, this engineered nanobiosystem holds promise as an effective treatment strategy with theranostic properties, capable of overcoming or mitigating resistance in KRAS mutant CRC cells.

Acknowledgments

The authors extend their gratitude to the Research Center for Pharmaceutical Nanotechnology, the Liver and Gastrointestinal Diseases Research Center, and the Department of Pharmaceutics, Faculty of Pharmacy at Tabriz University of Medical Sciences for the technical supports. This research was funded by Tabriz University of Medical Sciences (Grant# 68496, Grant# 67132).

Author Contributions

Maedeh Yousefi: Investigation, Hamed Farzi-Khajeh: Methodology. Mostafa Akbarzadeh-Khiavi: Conceptualization, Supervision, Writing - Review & Editing. Azam Safary: Conceptualization, Writing - Original Draft, Supervision Khosro Adibkia: Conceptualization, Supervision, Writing - Review & Editing.

Conflict of Interest

The authors declare that they have no conflict of interest.

References

1. El Zarif T, Yibirin M, De Oliveira-Gomes D, Machaalani M, Nawfal R, Bittar G, et al. Overcoming therapy resistance in colon cancer by drug repurposing. Cancers. 2022;14(9):2105. doi:10.3390/cancers14092105
2. Koustas E, Trifylli EM, Sarantis P, Papadopoulos N, Karapedi E, Aloizos G, et al. Immunotherapy as a therapeutic strategy for gastrointestinal cancer-current treatment options and future perspectives. Int J Mol Sci. 2022;23(12):6664. doi:10.3390/ijms23126664
3. Koveitypour Z, Panahi F, Vakilian M, Peymani M, Seyed Forootan F, Nasr Esfahani MH, Ghaedi K. Signaling pathways involved in colorectal cancer progression. Cell Biosci. 2019;9:97. doi:10.1186/s13578-019-0361-4
4. Akbarzadeh-Khiavi M, Farzi-Khajeh H, Somi MH, Safary A, Barar J, Ansari R, Omidi Y. Eradication of kras mutant colorectal adenocarcinoma by pegylated gold nanoparticles-cetuximab conjugates through ros-dependent apoptosis. Colloids Surf A: Physicochem Eng Asp. 2022;653:129890. doi:10.1016/j.colsurfa.2022.129890
5. Akbarzadeh Khiavi M, Safary A, Barar J, Farzi-Khajeh H, Barzegari A, Mousavi R, et al. Pegylated gold nanoparticles-ribonuclease induced oxidative stress and apoptosis in colorectal cancer cells. Bioimpacts. 2020;10(1):27-36. doi:10.15171/bi.2020.04
6. Yang J, Mo J, Dai J, Ye C, Cen W, Zheng X, et al. Cetuximab promotes rsl3-induced ferroptosis by suppressing the nrf2/ho-1 signalling pathway in kras mutant colorectal cancer. Cell Death Dis. 2021;12(11):1079. doi:10.1038/s41419-021-04367-3

7. Akbarzadeh-Khiavi M, Safary A, Omidi Y. Targeting long non-coding rnas as new modulators in anti-egfr resistance mechanisms. Bioimpacts 2024;14(1):27696. doi:10.34172/bi.2023.27696
8. Lee DY, Song MY, Kim EH. Role of oxidative stress and nrf2/keap1 signaling in colorectal cancer: Mechanisms and therapeutic perspectives with phytochemicals. Antioxidants (Basel). 2021;10(5):743. doi:10.3390/antiox10050743
9. Villalpando-Rodriguez GE, Gibson SB. Reactive oxygen species (ros) regulates different types of cell death by acting as a rheostat. Oxid Med Cell Longev. 2021;2021:9912436. doi:10.1155/2021/9912436
10. Lee YJ, Kim WI, Bae JH, Cho MK, Lee SH, Nam HS, et al. Overexpression of nrf2 promotes colon cancer progression via erk and akt signaling pathways. Ann Surg Treat Res. 2020;98(4):159-67. doi:10.4174/astr.2020.98.4.159
11. Snezhkina AV, Kudryavtseva AV, Kardymon OL, Savvateeva MV, Melnikova NV, Krasnov GS, Dmitriev AA. Ros generation and antioxidant defense systems in normal and malignant cells. Oxid Med Cell Longev. 2019;2019:6175804. doi:10.1155/2019/6175804
12. Basak D, Uddin MN, Hancock J. The role of oxidative stress and its counteractive utility in colorectal cancer (crc). Cancers. 2020;12(11):3336. doi:10.3390/cancers12113336
13. Bardelčíková A, Šoltys J, Mojžiš J. Oxidative stress, inflammation and colorectal cancer: An overview. Antioxidants (Basel). 2023;12(4):901. doi:10.3390/antiox12040901
14. Kim SJ, Kim HS, Seo YR. Understanding of ros-inducing strategy in anticancer therapy. Oxid Med Cell Longev. 2019;2019:5381692. doi:10.1155/2019/5381692
15. Perillo B, Di Donato M, Pezone A, Di Zazzo E, Giovannelli P, Galasso G, et al. Ros in cancer therapy: The bright side of the moon. Exp Mol Med. 2020;52(2):192-203. doi:10.1038/s12276-020-0384-2
16. Kim KS, Lee D, Song CG, Kang PM. Reactive oxygen species-activated nanomaterials as theranostic agents. Nanomedicine (Lond). 2015;10(17):2709-23. doi:10.2217/nnm.15.108
17. Arfin S, Jha NK, Jha SK, Kesari KK, Ruokolainen J, Roychoudhury S, et al. Oxidative stress in cancer cell metabolism. Antioxidants (Basel). 2021;10(5):642. doi:10.3390/antiox10050642
18. Fathi M, Safary A, Barar J. Therapeutic impacts of enzyme-responsive smart nanobiosystems. Bioimpacts. 2020;10(1):1-4. doi:10.15171/bi.2020.01
19. Akbarzadeh-Khiavi M, Torabi M, Olfati AH, Rahbarnia L, Safary A. Bio-nano scale modifications of melittin for improving therapeutic efficacy. Expert Opin Biol Ther. 2022;22(7):895-909. doi:10.1080/14712598.2022.2088277
20. Jain A, Bhattacharya S. Recent advances in nanomedicine preparative methods and their therapeutic potential for colorectal cancer: A critical review. Front Oncol. 2023;13:1211603. doi:10.3389/fonc.2023.1211603
21. Zhu L, Zhou Z, Mao H, Yang L. Magnetic nanoparticles for precision oncology: Theranostic magnetic iron oxide nanoparticles for image-guided and targeted cancer therapy. Nanomedicine (Lond). 2017;12(1):73-87. doi:10.2217/nnm-2016-0316
22. Shen L, Li B, Qiao Y. Fe_3O_4 nanoparticles in targeted drug/gene delivery systems. Materials (Basel). 2018;11(2):324. doi:10.3390/ma11020324
23. Włodarczyk A, Gorgoń S, Radoń A, Bajdak-Rusinek K. Magnetite nanoparticles in magnetic hyperthermia and cancer therapies: Challenges and perspectives. Nanomaterials. 2022;12(11): 1807. doi:10.3390/nano12111807
24. Hervault A, Thanh NT. Magnetic nanoparticle-based therapeutic agents for thermo-chemotherapy treatment of cancer. Nanoscale. 2014;6(20):11553-73. doi:10.1039/c4nr03482a
25. Luong D, Sau S, Kesharwani P, Iyer AK. Polyvalent folate-dendrimer-coated iron oxide theranostic nanoparticles for simultaneous magnetic resonance imaging and precise cancer cell targeting. Biomacromolecules. 2017;18(4):1197-209. doi:10.1021/acs.biomac.6b01885
26. Deng L, Li Q, Al-Rehili S, Omar H, Almalik A, Alshamsan A, et al. Hybrid iron oxide-graphene oxide-polysaccharides microcapsule: A micro-matryoshka for on-demand drug release and antitumor therapy in vivo. ACS Appl Mater Interfaces. 2016;8(11):6859-68. doi:10.1021/acsami.6b00322
27. Pramanik A, Jones S, Pedraza F, Vangara A, Sweet C, Williams MS, et al. Fluorescent, magnetic multifunctional carbon dots for selective separation, identification, and eradication of drug-resistant superbugs. ACS Omega. 2017;2(2):554-62. doi:10.1021/acsomega.6b00518
28. Voinov MA, Sosa Pagán JO, Morrison E, Smirnova TI, Smirnov AI. Surface-mediated production of hydroxyl radicals as a mechanism of iron oxide nanoparticle biotoxicity. J Am Chem Soc. 2011;133(1):35-41. doi:10.1021/ja104683w
29. Ahamed M, Alhadlaq HA, Alam J, Khan MA, Ali D, Alarafi S. Iron oxide nanoparticle-induced oxidative stress and genotoxicity in human skin epithelial and lung epithelial cell lines. Curr Pharm Des. 2013;19(37):6681-90. doi:10.2174/1381612811319370011
30. Xiong P, Huang X, Ye N, Lu Q, Zhang G, Peng S, et al. Cytotoxicity of metal-based nanoparticles: From mechanisms and methods of evaluation to pathological manifestations. Adv Sci. 2022;9(16):2106049. doi:10.1002/advs.202106049
31. Singh I, Pahan K, Khan M, Singh AK. Cytokine-mediated induction of ceramide production is redox-sensitive. Implications to proinflammatory cytokine-mediated apoptosis in demyelinating diseases. J Biol Chem. 1998;273(32):20354-62. doi:10.1074/jbc.273.32.20354
32. Reynolds MB, Hong HS, Michmerhuizen BC, Lawrence

AE, Zhang L, Knight JS, et al. Cardiolipin coordinates inflammatory metabolic reprogramming through regulation of complex ii disassembly and degradation. Sci Adv. 2023;9(5):eade8701. doi:10.1126/sciadv.ade8701
33. Min Y, Suminda GGD, Heo Y, Kim M, Ghosh M, Son YO. Metal-based nanoparticles and their relevant consequences on cytotoxicity cascade and induced oxidative stress. Antioxidants (Basel) 2023;12(3):703. doi:10.3390/antiox12030703
34. Farzi-Khajeh H, Jafari B, Safa KD, Dastmalchi S. Magnetic iron oxide nanoparticles modified with vanadate and phosphate salts for purification of alkaline phosphatase from the bovine skim milk. Colloids and surfaces B Biointerfaces. 2019;175:644-53. doi:10.1016/j.colsurfb.2018.12.051
35. Yu D, Zha Y, Zhong Z, Ruan Y, Li Z, Sun L, Hou S. Improved detection of reactive oxygen species by dcfh-da: New insight into self-amplification of fluorescence signal by light irradiation. Sens Actuators B Chem. 2021;339:129878. doi:10.1016/j.snb.2021.129878
36. Nakamura H, Takada K. Reactive oxygen species in cancer: Current findings and future directions. Cancer Sci. 2021;112(10):3945-52. doi:10.1111/cas.15068
37. Yusuf A, Almotairy ARZ, Henidi H, Alshehri OY, Aldughaim MS. Nanoparticles as drug delivery systems: A review of the implication of nanoparticles' physicochemical properties on responses in biological systems. Polymers. 2023;15(7):1596. doi:10.3390/polym15071596
38. Tarrés Q, Aguado R, Zoppe JO, Mutjé P, Fiol N, Delgado-Aguilar M. Dynamic light scattering plus scanning electron microscopy: Usefulness and limitations of a simplified estimation of nanocellulose dimensions. Nanomaterials. 2022;12(23):4288. doi:10.3390/nano12234288
39. Mu K, Zhang S, Ai T, Jiang J, Yao Y, Jiang L, et al. Monoclonal antibody-conjugated superparamagnetic iron oxide nanoparticles for imaging of epidermal growth factor receptor-targeted cells and gliomas. Mol Imaging. 2015;14(5):1-12. doi:10.2310/7290.2015.00002
40. Rieger AM, Nelson KL, Konowalchuk JD, Barreda DR. Modified annexin v/propidium iodide apoptosis assay for accurate assessment of cell death. J Vis Exp. 2011;50:2597. doi:10.3791/2597
41. Tseng SH, Chou MY, Chu IM. Cetuximab-conjugated iron oxide nanoparticles for cancer imaging and therapy. Int J Nanomedicine. 2015;10:3663-85. doi:10.2147/ijn.S80134
42. Gurer-Orhan H, Ince E, Konyar D, Saso L, Suzen S. The role of oxidative stress modulators in breast cancer. Curr Med Chem. 2018;25(33):4084-101. doi:10.2174/0929867324666170711114336
43. Gorrini C, Harris IS, Mak TW. Modulation of oxidative stress as an anticancer strategy. Nat Rev Drug Discov. 2013;12(12):931-47. doi:10.1038/nrd4002
44. Wang J, Yi J. Cancer cell killing via ros: To increase or decrease, that is the question. Cancer Biol Ther. 2008;7(12):1875-84. doi:10.4161/cbt.7.12.7067
45. Russell E, Dunne V, Russell B, Mohamud H, Ghita M, McMahon SJ, et al. Impact of superparamagnetic iron oxide nanoparticles on in vitro and in vivo radiosensitisation of cancer cells. Radiat Oncol. 2021;16(1):104. doi:10.1186/s13014-021-01829-y
46. Sadeghi MR, Jeddi F, Soozangar N, Somi MH, Samadi N. The role of nrf2-keap1 axis in colorectal cancer, progression, and chemoresistance. Tumour Biol. 2017;39(6):1010428317705510. doi:10.1177/1010428317705510
47. Rocha CR, Kajitani GS, Quinet A, Fortunato RS, Menck CF. Nrf2 and glutathione are key resistance mediators to temozolomide in glioma and melanoma cells. Oncotarget. 2016;7(30):48081-92. doi:10.18632/oncotarget.10129
48. Panieri E, Buha A, Telkoparan-Akillilar P, Cevik D, Kouretas D, Veskoukis A, et al. Potential applications of nrf2 modulators in cancer therapy. Antioxidants (Basel). 2020;9(3):193. doi:10.3390/antiox9030193